Uninephrectomy augments the effects of high fat diet induced obesity on gene expression in mouse kidney

Gai, Zhibo; Hiller, Christian; Chin, Siew Hung; Hofstetter, Lia; Stieger, Bruno; Konrad, Daniel; Kullak-Ublick, Gerd A

Abstract: Obesity has been reported as an independent risk factor for chronic kidney disease, leading to glomerulosclerosis and renal insufficiency. To assess the relationship between a reduced nephron number and a particular susceptibility to obesity-induced renal damage, mice underwent uninephrectomy (UNX) followed by either normal chow or high-fat diet (HFD) and were compared with sham-operated control mice. After 20 weeks of dietary intervention, HFD-fed control mice presented characteristic features of progressive nephropathy, including albuminuria, glomerulosclerosis, renal fibrosis and oxidative stress. These changes were more pronounced in HFD-fed mice that had undergone uninephrectomy. Analysis of gene expression in mouse kidney by whole genome microarrays indicated that high fat diet led to more changes in gene expression than uninephrectomy. HFD affected mainly genes involved in lipid metabolism and transport, whereas the combination of UNX and HFD additionally altered the expression of genes belonging to cytoskeleton remodeling, fibrosis and hypoxia pathways. Canonical pathway analyses identified the farnesoid X receptor (FXR) as a potential key mediator for the observed changes in gene expression associated with UNX-HFD. In conclusion, HFD-induced kidney damage is more pronounced following uninephrectomy and is associated with changes in gene expression that implicate FXR as a central regulatory pathway.

DOI: https://doi.org/10.1016/j.bbadis.2014.07.001

Uninephrectomy augments the effects of high fat diet induced obesity on gene expression in mouse kidney

Zhibo Gai[a], Christian Hiller [a], Siew Hung Chin[b,c,d], Lia Hofstetter [a], Bruno Stieger [a], Daniel Konrad[b,c,d], Gerd A. Kullak-Ublick [a,d,*]

[a] Department of Clinical Pharmacology and Toxicology, University Hospital Zurich, Switzerland
[b] Division of Pediatric Endocrinology and Diabetology and [c] Children's Research Centre, University Children's Hospital, Zurich, Switzerland; [d] Zurich Centre for Integrative Human Physiology, University of Zurich, Switzerland

E-Mail addresses:
zhibo.gai@usz.ch
christian.hiller@usz.ch
siewhung.chin@usz.ch
lia.hofstetter@usz.ch
bruno.stieger@uzh.ch
daniel.konrad@kispi.uzh.ch
gerd.kullak@usz.ch

Abbreviated title: Effect of uninephrectomy on high fat diet induced renal damage

* Corresponding author:

Gerd A. Kullak-Ublick, M.D.
Department of Clinical Pharmacology and Toxicology
University Hospital Zurich
Rämistrasse 100
CH-8091 Zurich / Switzerland
Tel.: + 41 44 255 2068
Fax: + 41 44 255 9676
Email: gerd.kullak@usz.ch

Abstract

Obesity has been reported as an independent risk factor for chronic kidney disease, leading to glomerulosclerosis and renal insufficiency. To assess the relationship between a reduced nephron number and a particular susceptibility to obesity-induced renal damage, mice underwent uninephrectomy (UNX) followed by either normal chow or high-fat diet (HFD) and were compared with sham-operated control mice. After 20 weeks of dietary intervention, HFD-fed control mice presented characteristic features of progressive nephropathy, including albuminuria, glomerulosclerosis, renal fibrosis and oxidative stress. These changes were more pronounced in HFD-fed mice that had undergone uninephrectomy. Analysis of gene expression in mouse kidney by whole genome microarrays indicated that high fat diet led to more changes in gene expression than uninephrectomy. HFD affected mainly genes involved in lipid metabolism and transport, whereas the combination of UNX and HFD additionally altered the expression of genes belonging to cytoskeleton remodeling, fibrosis and hypoxia pathways. Canonical pathway analyses identified the farnesoid X receptor (FXR) as a potential key mediator for the observed changes in gene expression associated with UNX-HFD. In conclusion, HFD-induced kidney damage is more pronounced following uninephrectomy and is associated with changes in gene expression that implicate FXR as a central regulatory pathway.

Keywords: gene regulation; nuclear receptor; bile acids; organic anion transporter; Wnt signaling, BMP pathway

Abbreviations: UNX: uninephrectomy; HFD: high fat diet; FXR: farnesoid X receptor; CKD: chronic kidney disease; OATP, organic anion transporting polypeptide; OAT, organic anion transporter; SLC/Slc, solute carrier gene family; Abc, ATP-binding cassette transporter

1. Introduction

Obesity is not only associated with an increase in morbidity, mortality and reduction in life expectancy, but also leads to an increase in the incidence of diabetes, hypertension and dyslipidemia [1, 2]. Furthermore, obesity is now being increasingly recognized as a major and independent risk factor for the development of chronic kidney disease (CKD) [3, 4], focal glomerulosclerosis [5], and end stage renal disease (ESRD) [6-9]. Recent observational studies demonstrate that obesity is an independent risk factor for CKD in patients with reduced renal mass [6, 9]. Currently, a growing population lives with reduced renal mass considering the higher rates of primary kidney tumor in adults and congenital solitary kidney in children, as well as the rising number of living kidney donors [10-13]. Given the epidemics of overweight in the U.S. and worldwide [14, 15], the number of obese people with reduced renal mass is expected to increase. Despite the public health and clinical implications of the relationships between obesity and kidney injury in patients that have undergone nephrectomy [6, 9], the mechanisms leading to obesity-induced renal damage in reduced renal mass are less clear.

To date, clinical and experimental studies have shown that the characteristic features of obesity induced kidney injury [16, 17] contribute to albuminuria, a progressive decline in renal function and ultimately glomerulosclerosis and tubulointerstitial fibrosis [18-22]. Since chronic kidney disease is a complex kidney disease, interruption of a single pathway is unlikely to result in a significant therapeutic benefit. Further understanding of the pathogenesis of renal failure thus requires global expression analysis of disease states using genomics and/or proteomics tools [23-27].

In this study, high-fat-diet-fed mice were used as an obesity model. We examined kidney function and histological changes of 20-week uninephrectomized (UNX) mice fed a chow diet (UNX-chow), UNX mice fed a high fat diet (UNX-HFD) and sham-operated control mice (Sham-chow and Sham-HFD). Gene expression in kidney tissue of these four groups was also analyzed to better comprehend the molecular mechanisms underlying advanced renal disease and the pathogenetic role of obesity in the onset of proteinuria and renal insufficiency. UNX-HFD mice presented higher degrees of progressive nephropathy, albuminuria and renal fibrosis. Moreover, we observed marked changes in a number of genes and gene families involved in cytoskeleton remodeling, fibrosis and lipid metabolism in the UNX-HFD group and novel pathways linked with farnesoid X receptor (FXR) signaling that have not been previously associated with renal disease progression. The altered expression of some of these genes is also associated with possible protective and compensatory mechanisms. Additionally, our results indicate that obesity-induced chronic renal disease is accelerated in UNX.

2. Materials and Methods

2.1 Uninephrectomy

Male C57/BJ mice aged 6 weeks were randomly assigned to uninephrectomy (UNX) or sham procedures and fed with a high fat diet (D12331; ResearchDiets, NJ, USA) or control chow diet (Provimi Kliba). Mice were divided into 4 groups of 6: Sham-chow, UNX-chow, Sham-HFD and UNX-HFD. For uninephrectomy, mice were initially anesthetized with 3% to 5% isoflurane, orally intubated, and mechanically ventilated. Anesthesia was maintained with 1.5% to 2% isoflurane delivered in oxygen. The left kidney was surgically removed via a left paramedian incision on the back. The adrenal gland was carefully freed from the upper pole of the renal capsule before the renal pedicle was ligated and the kidney removed. For sham surgery, the kidney was manipulated without ablation. All mice were sacrificed under anesthesia 20 weeks after surgery and kidneys were harvested. Half of the kidney from each animal was snap frozen in liquid nitrogen and stored at -80°C for RNA and protein extraction. The other half was fixed with formalin for histology. All protocols conformed to the Swiss animal protection laws and were approved by the Cantonal Veterinary Office in Zurich, Switzerland.

2.2 Measurement of plasma and urine samples

For 24-hour urine collection, individual mice were placed in metabolic cages with access to diets. Urinary albumin and creatinine concentrations were measured with the Albumin mouse ELISA kit (ab108792, Abcam, Cambridge, UK) and Creatinine assay kit (ab65340, Abcam, Cambridge, UK). Urinary H_2O_2 levels were measured using the Amplex Red H_2O_2 assay kit (A12214, Invitrogen, CA, US). Plasma samples were obtained from tail blood of fasted mice. Plasma cholesterol and triglyceride levels were measured by the Amplex Red cholesterol assay kit (A12216, Invitrogen, CA, US) and theTriglyceride assay kit (ETGA-200, EnzyChrom, Aachen, Germany), respectively.

2.3 Assessment of renal pathology and immunostaining

Kidneys were fixed overnight in 10% neutral buffer formalin and embedded in paraffin. Tissue sections were cut at 3 µm and stained for hematoxylin and eosin, periodic acid-Schiff (PAS) and Masson's trichrome using standard protocols. Mesangial area was determined from PAS stained sections and fibrotic area was assessed from trichrome stained sections as described [28, 29]. Briefly, digital images of random high power fields were analyzed by a blind observer. The cross-sectional area of the glomerulus or area of fibrosis was determined by using the program Adobe Photoshop. 4 mice were analyzed per group. Immunostaining was performed on paraffin sections using a microwave based antigen retrieval technique. The antibodies used in this study included Actn1 (Novus biologicals, Cambridge, UK), Slc27a4 (Proteintech, Manchester, UK), TNFα (Abcam, Cambridge, UK) and Cyp4a (Santa Cruz, CA, US). The antibody against Slco1a1 was previously raised in our group (Dr. Bruno Stieger). Sections were treated with the Envision$^+$ DAB kit (Dako, Denmark) according to the manufacturer's instruction.

2.4 Microarray and gene expression analysis

RNA was extracted from frozen kidney using RNeasy Microarray Tissue mini kit (73304, Qiagen, Germany), followed by on column DNase digestion to remove any contaminating genomic DNA. RNA samples from 4 mice per group were subjected to microarray analysis. Briefly, 100 ng of total RNA was reverse-transcribed into double-stranded cDNA, which was linearly amplified and labelled with Cy3 dye. Following quantification using a Nanodrop spectrophotometer (Witec, Luzern, Switzerland) and quality assessment with Agilent 2100 Bioanalyzer (Agilent Technologies, Santa Clara, CA), 1.6 µg of the obtained Cy3-labeled cRNA was hybridized to Mouse GE 4x44K v2 Microarrays (Agilent Technologies, Santa Clara, CA) according to the manufacturer's protocol. Arrays were scanned with an Agilent G2565CA Microarray Scanner System (Agilent, Santa Clara, CA). Raw intensity data were obtained

using Agilent's Feature Extraction Software *version 10.7* for array image analysis and the calculation of spot intensity measurements. Data analysis was carried out with R/Bioconductor. The processed intensities and normalized across samples were loaded by using quantile normalization. All microarray data was submitted to the Gene Expression Omnibus (accession number GSE53996). Differential expression was computed using the *limma* package. More details on analysis methods can be found at http://fgcz-bfabric.uzh.ch/wiki/tiki-index.php?page=app.two_groups. Gene oncology analysis, network analysis and canonical pathway analysis of the microarray data were completed using the Ingenuity Pathway Analysis (Qiagen, Redwood, CA) software, MetaCore online service (Thomson Reuters), and Subio platform (Subio Inc, Kagoshima, Japan).

2.5 Semi-quantitative RT-PCR

Validation of microarray data was performed for selected differentially expressed genes by sqRT-PCR. Briefly, 2 µg total RNA (n = 3 to 4), from the same samples sent for microarray, was reverse transcribed using oligo-dT priming and SuperscriptII (Invitrogen, CA, US). First-strand complementary DNA was used as the template for real-time polymerase chain reaction analysis with TaqMan master mix and primers (Applied Biosystems, CA, US). Transcript levels, determined in two independent complementary DNA preparations, were calculated as described and expressed relative to villin as housekeeping gene.

2.6 Statistical analyses

Data are expressed as mean ± SEM. For microarray data, comparison was assessed by student's *t* test with R/Bioconductor to generate differentially expressed genes (UNX-Chow vs. Sham-Chow; UNX-HFD vs. Sham-HFD; Sham-HFD vs. Sham-Chow; UNX-HFD vs. UNX-Chow). For other data regarding to baseline characteristic analysis and histological analysis, comparison between groups was assessed by one-way ANOVA followed by Bonferroni's test. Statistical analyses were performed with GraphPad software.

2.7 Supplementary material

The following supplementary information is available online:

Table S1. Differentially expressed genes (≥ 1.7 fold) in 20-week sham-HFD kidneys as compared with sham-chow kidneys

Table S2. Differentially expressed genes (≥ 1.7 fold) in 20-week remnant UNX-HFD kidneys as compared with UNX-chow kidneys

Table S3. Genes differentially expressed in both UNX and sham-operated mice fed a high fat diet (≥ 1.7 fold, $p<0.05$)

Table S4. Genes that show a change in expression level only in UNX-HFD remnant kidneys (≥ 1.7 fold, $p<0.05$)

Table S5. Formula of high fat diet #D12331

Figure S1. Thin layer chromatography (TLC) results of kidney lipid composition. (A, B) Representative images taken from TLC results. Quantitative analyses of total phospholipids (C) and cholesterol (D) from each group (n = 4 / group, data represent mean ± SEM).

Supplementary method. Thin layer chromatography

3. Results

3.1 Systemic metabolic abnormalities

To evaluate the effect of uninephrectomy (UNX) on HFD-induced renal disease, mice at six weeks of age underwent UNX, followed by either a normal or high fat diet (HFD) for 20 weeks. The characteristics of the four groups at 20 weeks of the experimental period are presented in Table 1. Both sham and UNX mice that consumed HFD showed markedly increased body weight. The body weight of UNX-chow and UNX-HFD mice tended to be lower than in their counterparts that had undergone sham operation, although this difference did not reach statistical significance during the observation period. UNX significantly increased the weight of the remnant kidney, especially in mice fed the HFD. Mice from the HFD group showed significantly higher plasma triglyceride and cholesterol levels. UNX, however, had no effects on these biochemical parameters. As shown in Fig. 1, the biochemical analysis of creatinine and albumin confirmed chronic renal disease progression in UNX-HFD mice. Sham-operated mice consuming the HFD developed progressive albuminuria and UNX produced a more striking increase in the albumin/creatinine ratio in mice fed the HFD at 20 weeks. Moreover, the urinary H_2O_2 level was also significantly higher in the UNX group after 20 weeks of the high fat diet, indicating a greater degree of oxidative stress in the UNX-HFD remnant kidney.

3.2 UNX accelerates renal fibrosis and glomerulosclerosis in obese mice

The effect of UNX on the acceleration of fibrosis and glomerulosclerosis in obese mice was evident by trichrome and PAS staining. As shown in Fig. 2, HFD increased fibrosis in sham-operated mice assessed after 20 weeks of feeding (Fig. 2 G). However, kidney sections from UNX-HFD mice showed the most severe degree of fibrosis (Fig. 2 H). By quantitative analysis (Fig. 2 M), interstitial fibrosis, as determined by Trichrome staining, was approximately 2-fold greater in UNX-HFD kidneys than in Sham-HFD kidneys. Furthermore, quantitation from PAS-stained sections showed that the mesangial matrix content was increased significantly by UNX in HFD kidneys compared with the sham-operated counterparts (Fig. 2 I-L and N).

3.3 Effects of UNX and HFD on gene expression in the kidney

In parallel, global gene expression in the 20-week remnant kidneys of uninephrectomized mice fed either a chow or a high fat diet was compared with kidney tissue from the corresponding sham groups. 3-4 total RNA samples per group were analyzed and gene expression was compared between groups.

First, gene expression was compared between UNX-chow mice versus sham-chow mice (UNX-chow/Sham-chow) and between UNX-HFD mice versus sham-HFD mice (UNX-HFD/Sham-HFD). By using a ≥ 1.7-fold change as a cut-off, only 157 genes were differentially expressed between the UNX-chow/Sham-chow groups and 136 genes between the UNX-HFD/Sham-HFD groups (Fig. 3 A). Analysis of plot sources of variation confirmed that the impact of the high fat diet was greater than that of UNX on gene expression in these four groups (Fig. 3 B).

Next, in order to identify genes altered by HFD, the following datasets were compared: UNX-HFD versus UNX-chow (designated as UNX dataset) and sham-HFD versus sham-chow (designated as sham dataset). Comparison of data from Sham-HFD versus Sham-chow and data from UNX-HFD versus UNX-chow revealed that 2441 and 2581 genes, respectively, were significantly increased or decreased at least 1.7-fold (Fig. 3 A, Tables S1 and S2). Interestingly, a substantial number of genes (1289 genes) overlapped in being differentially expressed in both the UNX-HFD/UNX-chow and the sham-HFD/sham-chow datasets, as shown by Venn diagram analysis (Fig. 4 A and Table S3). The overlapping genes in both the UNX and sham datasets included genes involved in lipid transport and metabolism (Fig. 4 B). However, genes implicated in ion transport and in renal hypoxia showed altered expression only in the

UNX-HFD remnant kidneys (Fig. 4 C, Table 3 and Table S4). Importantly, the altered expression of genes responsive to hypoxia (Table 3) is consistent with the increased urinary H_2O_2 levels in UNX-HFD mice.

The differences between the two datasets were further confirmed by network and canonical pathway analyses. Network analyses with these two datasets are shown in Fig. 5. The common networks from both datasets were associated with cell adhesion, inflammation and apoptosis, whereas networks linked to cytoskeleton remodeling and cell-matrix adhesion mainly fell into the UNX dataset. Table 2 shows the discrepancies between the canonical pathways in each dataset. The FXR pathway is the top canonical pathway in the UNX-HFD dataset with 14 genes altered 1.7-fold, whereas only 10 genes are significantly changed in the Sham-HFD dataset (Table 3). Several canonical pathways which relate to fibrogenesis were also shown to be significantly changed in the UNX dataset, including decreased expression of genes within the BMP pathway and increased expression of genes within the Wnt signaling pathway (Table 3), which is in line with the histological observations (Fig. 2 H and M).

3.4 Validation of microarray findings with semi-quantitative RT-PCR and immunostaining

To validate microarray results, we selected 9 FXR-regulated genes in the UNX dataset and quantified their expression by real-time PCR. All sqRT-PCR analyses were performed in samples previously used for microarray experiments. We found that both methods (microarray analysis and sqRT-PCR) yielded similar results regarding the increase and decrease in gene expression (Fig. 6).

Next, we examined the immunostaining of kidney sections with specific antibodies against Actn1, Slco1a1, Slc27a4, TNFα and Cyp4a. Figure 7 shows representative staining images of kidney sections from different treatment groups. Consistent with the changes in gene expression shown in Fig. 6 and Table 3, the staining of Actn1 (actinin, a cytoskeletal protein, 3.2-fold increase at the mRNA level) was increased in the cytoplasm of tubular cells (mostly proximal tubules) in the UNX-HFD group (Fig. 7A-7D); staining of Slc27a4 (fatty acid transporter 4, 1.9-fold increase at the mRNA level) was enhanced in the apical membrane of proximal tubules (indicated by arrows, Fig. 7I-7L); staining of TNFα (4.35-fold increase at the mRNA level) and Cyp4a14 (2.3-fold increase at the mRNA level) was increased in the cytoplasm of tubular cells (indicated by arrows, Fig. 7M-7P and 7Q-7T, respectively). In contrast, staining of Slco1a1 (Oatp1a1, organic anion transporter that mediates the reuptake of organic anions, 0.36-fold decrease at mRNA level) was decreased in the apical membrane of proximal tubules in UNX-HFD kidney sections (Fig. 7E-7H).

4. Discussion

An emerging body of evidence suggests that obesity is not only a risk factor for CKD, but also an independent cause of renal dysfunction. Glomerulosclerosis and progressive renal insufficiency have been reported in obese patients and experimental animals with a normal renal mass [5, 30]. Therefore, it is conceivable that renal damage due to obesity-related hyperfiltration is especially severe in conjunction with a reduction in renal mass. Studies on the relationship between reduced nephron number and susceptibility to obesity-related renal damage have suggested that obesity is associated with higher glomerular hyperfiltration [31] and higher risks of proteinuria and CKD [9, 32] in kidney donors. These observations led us to explore the mechanisms underlying renal insufficiency after renal mass reduction. We showed that obesity has marked effects on proteinuria, glomerular damage and interstitial fibrosis in mice fed a HFD, and these changes were further enhanced by uninephrectomy. Furthermore, gene profiling analysis and functional classification of differentially expressed genes in kidneys from each group revealed the synergistic effects of UNX and HFD on the expression of genes responsible for cytoskeletal morphogenesis, fibrosis and lipid metabolism. As a consequence, the function of the remnant kidney is more severely impaired.

The gene profiling results are partly consistent with other studies analyzing gene expression in obesity-related glomerulopathy in obese patients [17]. One important group of genes with a notable change in expression induced by the high fat diet involved lipid metabolism and transport, in both Sham-HFD and UNX-HFD groups. Disturbances in lipid metabolism are often observed in patients with chronic renal failure, and the negative impact of proteinuria on kidney disease progression could be mediated in part through the increased filtration of lipoproteins [33]. Network analysis showed that more genes involved in lipid transport and metabolism were affected in obese mice than in mice fed the chow diet (Table 3). Furthermore, several other networks were identified to be uniquely expressed in the UNX-HFD dataset, including cytoskeleton remodeling, cell-matrix adhesion and other genes involved in fibrogenesis. Thus, our microarray data are consistent with histological results which indicate that kidneys from UNX-HFD mice have a higher degree of mesangial matrix content and interstitial fibrosis.

Pathway analysis implicated the Fxr signaling pathway as showing the strongest degree of activation in the remaining kidney of UNX-HFD mice. Fxr plays crucial roles in bile acid, cholesterol, lipid and glucose metabolism in the liver and intestine. In the liver, Fxr activation exerts antifibrotic effects by increasing the apoptosis of hepatic stellate cells [34]. However, the role of Fxr in kidney disease is still unclear. Fxr activation by potent agonists protects kidney function and limits renal fibrosis in diabetic and obese mice [35-37]. We previously showed that incubation of primary cultured rat renal proximal tubular cells with the FXR ligand chenodeoxycholic acid regulates the expression of bile acid transporters [38]. Moreover, exposure of hepatoma cells to bile acids decreased expression of hOATP1B1 (SLCO1B1) and hOAT2 (SLC22A7) by an FXR-mediated mechanism [39, 40]. Here, we show decreased renal expression of the orthologous mouse genes Slco1b2 and Slc22a7 (Fig. 6), suggesting a conserved role of Fxr in regulating bile acid transport in the kidney. However, recent studies on Fxr null mice with bile duct ligation show that loss of Fxr in fact protects the kidney from cholemic nephropathy caused by high plasma bile acids [41]. Future studies on kidney-specific Fxr knockout mice will be required to define the exact role of Fxr in obesity-induced kidney disease.

Whereas some diets commonly used to induce alterations in lipid homeostasis and/or obesity contain cholic acid to enhance fat absorption, the high fat diet D12331 used in the present study (formula shown in Table S5) did not contain bile acids. Thus, the effects on Fxr signaling seen in the UNX-HFD mice were not induced by external bile acid administration. UNX-HFD mice had a tendency towards increased plasma bile acid levels, however this increase did not reach statistical significance by ANOVA analysis

(data not shown). Because HFD has been reported to contribute to a dysfunction of the lysosomal system and altered lipid metabolism, characterized by cholesterol and phospholipid accumulation in the kidney [42], we also measured kidney lipid composition in each group by thin layer chromatography. UNX-HFD kidney tissue had a tendency towards increased total phospholipid and cholesterol content, although the differences between groups did not reach statistical significance by ANOVA analysis (Supplementary Fig. 1A-1D).

Nephrectomy in man is generally considered to have a favorable long-term outcome. To what degree a reduced renal mass is safe may depend, however, on the general health condition [43]. Our study, among various similar studies in a large variety of models for hypertension, diabetes and kidney disease [29, 44, 45], illustrates that in a diseased animal (including man), or in an animal model with increased glomerular capillary pressure, a reduction in renal mass is accompanied by an acceleration of renal disease. Taking into account the synergistic effects of obesity and UNX on the progression of renal insufficiency, avoidance of weight gain or weight loss in obese patients should be recommended to individuals with reduced renal mass [46-48]. Our results also have relevance in the setting of kidney donation, which results in a reduced renal mass and is being performed in an increasingly obese population [49].

In conclusion, we found that the effects of a HFD on the kidney appear to be accentuated in mice that have undergone uninephrectomy, as evidenced by accelerated progression of proteinuria and renal insufficiency 20 weeks after the procedure. This was also confirmed by the increased mesangial basement membrane area and the degree of renal fibrosis in the UNX-HFD mice. We thus show that uninephrectomy acts in synergism with HFD to promote changes in gene expression that are associated with renal damage and that activation of the FXR signaling pathway could be a protective mechanism in this model of advanced renal disease.

5. Acknowledgements

This study was supported by grant no. 320030_144193 from the Swiss National Science Foundation, the Swiss National Center for Competence in Research NCCR-Kidney.ch (to GAKU and DK), and the International Fellowship Program (grant no. 246539) on Integrative Kidney Physiology and Pathophysiology (IKPP).

6. Disclosure

All the authors declared no competing interests.

Figure Captions

Figure 1. **Albuminuria and urinary H_2O_2 output in the four treatment groups.** (A) Urine albumin/creatinine ratio increases with HFD at 20 weeks. (B) Urine H_2O_2/creatinine level is increased in mice fed with HFD for 20 weeks. Data are shown as mean ± SEM, * $p < 0.05$

Figure 2. **Histological analysis of remnant kidney tissue.** Histological appearance of glomeruli in (A) Sham-chow mice, (B) UNX-chow mice, (C) Sham-HFD mice and (D) UNX-HFD mice. Representative images of (E to H) Masson trichrome-stained and (I to L) PAS stained renal sections of kidney tissues of (E and I) Sham-chow mice, (F and J) UNX-chow mice, (G and K) Sham-HFD mice and (H and L) UNX-HFD mice. (M and N) Bars represent the quantitative analysis of (M) area of fibrosis and (N) area of mesangium where data are expressed as the mean ± SEM, * $p < 0.05$

Figure 3. **Microarray analysis of mRNA expression levels in kidney tissue of the four treatment groups.** (A) Summary of differentially expressed genes between groups. Cut off 1.7-fold, $p<0.05$. (B) Plot sources of variation analysis indicates diet as the factor with the higher impact on gene expression among those four groups. *Error* indicates no impact on gene expression. Data were analyzed using Subio platform software.

Figure 4. **Comparison of common and distinct gene expression patterns across the different experimental conditions.** (A) Venn diagram analysis of sham versus UNX datasets indicates that 1289 genes (green) are commonly expressed in both sham-HFD and UNX-HFD kidneys, whereas 1152 and 1292 genes are distinctly expressed in sham-HFD kidneys (blue) or UNX-HFD kidneys (orange), respectively. Data were analyzed using Subio platform software. (B) Gene ontology (GO) analysis of genes with a change in expression of ≥ 1.7 fold in kidney tissue of both Sham-HFD and UNX-HFD mice. Top 5 GO functional gene clusters are mostly involved in lipid transport and metabolism (green bars). (C) GO analysis of genes that showed a change of expression of ≥ 1.7 fold only in kidney tissue of UNX-HFD mice (orange bars).

Figure 5. **Network analysis of genes with a change of expression of ≥ 1.7 fold across treatment groups.** The top 5 networks are listed. Green bars indicate genes with a change of expression level in kidneys of both Sham-HFD and UNX-HFD mice; genes that show altered expression exclusively in kidney tissue of either Sham-HFD or UNX-HFD mice are indicated by blue and orange bars, respectively.

Figure 6. **sqRT- PCR validation of microarray data.** Changes in the expression level of FXR regulated genes as determined by microarray analysis (see Table 3) were reproducible by sqRT-PCR. Cyp4a14 is shown as a positive control for a HFD-induced increase in gene expression. Numbers shown in *italics* below gene names indicate the fold change in expression level detected by microarray (Table 3). Data are shown as mean ± SEM, * $p < 0.05$

Figure 7. **Immunohistochemistry staining of remnant kidney tissue for selected targets.** Kidney paraffin sections from different treatment groups were immunostained with antibodies against Actn1 (A to D), Slco1a1 (E to H, decreased expression in UNX-HFD), Slc27a4 (I to L), TNFα (M to P) and Cyp4a14 (Q to T). Arrows indicate positive staining shown in representative images.

Table 1: Baseline characteristics of the different treatment groups

	Sham		UNX	
	Chow	HFD	Chow	HFD
Body weight (g)	35.5±0.6	53.2±1.5*	33.7±0.8	47.5±3.1*
Kidney weight (mg)	215.0±9.0	235.8±8.9	272.0±11.5[§]	277.6±12.8[§]
Plasma TG (mg/dl)	97.0±14.0	139.6±12.1*	102.1±7.7	148.6±9.3*
Plasma Ch (mg/dl)	115.8±14.8	198.2±4.1*	109.4±5.8	177.9±15.5*

Abbreviations: UNX, uninephrectomy; HFD, high fat diet. n=6 mice/group. * $p < 0.05$, comparison between chow and HFD; [§]$p < 0.05$, comparison between Sham and UNX

Table 2: Top 5 canonical pathways from UNX-HFD dataset

Top 5 pathways by IPA (Ingenuity Pathway Analysis)		Top 5 pathways by MetaCore™	
Name	*p* value	Name	*p* value
FXR/RXR activation	3.11E-05	WNT and cytoskeletal remodeling	5.54E-08
LXR/RXR activation	2.86E-03	Neurophysiological process signaling	3.30E-05
Caveolar-mediated endocytosis signaling	4.35E-03	Cytoskeleton remodeling	2.43E-04
Androgen biosynthesis	4.4E-03	Cell-matrix glycoconjugates	1.02E-03
Retinoate biosynthesis	5.26E-03	Fxr regulated cholesterol and bile acid transport	1.62E-03

Differences in gene expression between UNX-HFD and UNX-chow groups were analyzed by IPA (Ingenuity Pathway Analysis) software and MetaCore™ pathway online analysis

Table 3: Selected differentially expressed genes (≥1.7 fold) in 20-week remnant kidney of UNX-HFD mice grouped according to function

Cytoskeleton remodeling
Actn1 (1.69), Cfl1 (1.33), Mmp7(1.68), Cd44(0.85), Hrh4(0.85), Taok2(1.54), Rap1a (1.91), Prkd3 (0.82), Tesk2 (0.77), Actg1 (0.98), Tubb3(1.65), Parva (0.79), Pfn1 (0.94)
Wnt signaling induced EMT (pro- fibrosis)
Wnt1 (0.79), Wnt16 (0.98), Trp73(1.12), Adam17(1.36), Adam25(0.81), Lfng (1.59), Actn1 (1.69), Actg1 (0.98), Dvl2 (0.96), Mmp7 (1.68)
Lipid metabolism
Abcb4 (-0.97), CYP2B10(-2.24), CYP2D10(-2.03), CYP3A59(-2.35), CYP4A32(1.16), Cyp7b1(-1.15), FOXO4(1.14), Mup1 (includes others), Nr1i3/Car(0.78), SLC1A6 (1.34), SLC27A4(0.95)
Response to hypoxia
Nppa (0.767), Ascl2 (0.8), Hpx (-3.54), Ece1 (0.85), Ccr6 (1.4), Ccr10 (1.07), Ppyr1 (0.95), Hif3a (1.39), Pklr (1.51), Kcna5 (1.42), Lep (2.63), Lepr (-0.84), P2rx2 (0.84), Pde7b (-0.82), Prkd3 (0.82), Pklr (1.51), Ramp1 (0.80), Ucp3 (1.26), Chrnb2 (0.84)
Fxr regulated transporters
Slco1a1 (-1.48), Slco1b2 (-2.53), Slc22a7 (-2.18), Abcb4 (-0.97)
Salt and fluid retention
Cyp4a14 (1.18), Slc4a4 (3.94), Slc9a3 (0.79)

Numbers in parentheses indicate gene expression levels quantified as Log2 of fold changes: (1.69) corresponds to a 3.23 fold, (-2.18) to a 0.22 fold change in gene expression

References

[1] H.Y. Cheng, Midlife body mass index and total mortality, JAMA, 295 (2006) 1772; author reply 1772.

[2] F.B. Hu, W.C. Willett, T. Li, M.J. Stampfer, G.A. Colditz, J.E. Manson, Adiposity as compared with physical activity in predicting mortality among women, N Engl J Med, 351 (2004) 2694-2703.

[3] M. Praga, E. Morales, Obesity, proteinuria and progression of renal failure, Curr Opin Nephrol Hypertens, 15 (2006) 481-486.

[4] Y. Wang, X. Chen, Y. Song, B. Caballero, L.J. Cheskin, Association between obesity and kidney disease: a systematic review and meta-analysis, Kidney Int, 73 (2008) 19-33.

[5] N. Kambham, G.S. Markowitz, A.M. Valeri, J. Lin, V.D. D'Agati, Obesity-related glomerulopathy: an emerging epidemic, Kidney Int, 59 (2001) 1498-1509.

[6] E. Gonzalez, E. Gutierrez, E. Morales, E. Hernandez, A. Andres, I. Bello, R. Diaz-Gonzalez, O. Leiva, M. Praga, Factors influencing the progression of renal damage in patients with unilateral renal agenesis and remnant kidney, Kidney Int, 68 (2005) 263-270.

[7] J.E. Hall, E.D. Crook, D.W. Jones, M.R. Wofford, P.M. Dubbert, Mechanisms of obesity-associated cardiovascular and renal disease, Am J Med Sci, 324 (2002) 127-137.

[8] C.Y. Hsu, C.E. McCulloch, C. Iribarren, J. Darbinian, A.S. Go, Body mass index and risk for end-stage renal disease, Annals of internal medicine, 144 (2006) 21-28.

[9] M. Praga, E. Hernandez, J.C. Herrero, E. Morales, Y. Revilla, R. Diaz-Gonzalez, J.L. Rodicio, Influence of obesity on the appearance of proteinuria and renal insufficiency after unilateral nephrectomy, Kidney Int, 58 (2000) 2111-2118.

[10] K. Akl, The anomalies associated with congenital solitary functioning kidney in children, Saudi J Kidney Dis Transpl, 22 (2011) 67-71.

[11] R. Dhote, N. Thiounn, B. Debre, G. Vidal-Trecan, Risk factors for adult renal cell carcinoma, Urol Clin North Am, 31 (2004) 237-247.

[12] M. Hiraoka, H. Tsukahara, Y. Ohshima, K. Kasuga, Y. Ishihara, M. Mayumi, Renal aplasia is the predominant cause of congenital solitary kidneys, Kidney Int, 61 (2002) 1840-1844.

[13] D.A. Mandelbrot, M. Pavlakis, Living donor practices in the United States, Adv Chronic Kidney Dis, 19 (2012) 212-219.

[14] C.L. Ogden, M.D. Carroll, L.R. Curtin, M.A. McDowell, C.J. Tabak, K.M. Flegal, Prevalence of overweight and obesity in the United States, 1999-2004, JAMA, 295 (2006) 1549-1555.

[15] M. Raj, R.K. Kumar, Obesity in children & adolescents, Indian J Med Res, 132 (2010) 598-607.

[16] T.M. Coimbra, U. Janssen, H.J. Grone, T. Ostendorf, U. Kunter, H. Schmidt, G. Brabant, J. Floege, Early events leading to renal injury in obese Zucker (fatty) rats with type II diabetes, Kidney Int, 57 (2000) 167-182.

[17] Y. Wu, Z. Liu, Z. Xiang, C. Zeng, Z. Chen, X. Ma, L. Li, Obesity-related glomerulopathy: insights from gene expression profiles of the glomeruli derived from renal biopsy samples, Endocrinology, 147 (2006) 44-50.

[18] K. Gotoh, M. Inoue, T. Masaki, S. Chiba, K. Shiraishi, T. Shimasaki, K. Matsuoka, H. Ando, K. Fujiwara, N. Fukunaga, K. Aoki, T. Nawata, I. Katsuragi, T. Kakuma, M. Seike, H. Yoshimatsu, Obesity-related chronic kidney disease is associated with spleen-derived IL-10, Nephrol Dial Transplant, 28 (2013) 1120-1130.

[19] A.E. Decleves, A.V. Mathew, R. Cunard, K. Sharma, AMPK mediates the initiation of kidney disease induced by a high-fat diet, J Am Soc Nephrol, 22 (2011) 1846-1855.

[20] S. Kume, T. Uzu, S. Araki, T. Sugimoto, K. Isshiki, M. Chin-Kanasaki, M. Sakaguchi, N. Kubota, Y. Terauchi, T. Kadowaki, M. Haneda, A. Kashiwagi, D. Koya, Role of altered renal lipid metabolism in the development of renal injury induced by a high-fat diet, J Am Soc Nephrol, 18 (2007) 2715-2723.

[21] A. Odermatt, The Western-style diet: a major risk factor for impaired kidney function and chronic kidney disease, Am J Physiol Renal Physiol, 301 (2011) F919-931.
[22] K. Stemmer, D. Perez-Tilve, G. Ananthakrishnan, A. Bort, R.J. Seeley, M.H. Tschop, D.R. Dietrich, P.T. Pfluger, High-fat-diet-induced obesity causes an inflammatory and tumor-promoting microenvironment in the rat kidney, Dis Model Mech, 5 (2012) 627-635.
[23] S.K. Bhavnani, F. Eichinger, S. Martini, P. Saxman, H.V. Jagadish, M. Kretzler, Network analysis of genes regulated in renal diseases: implications for a molecular-based classification, BMC Bioinformatics, 10 Suppl 9 (2009) S3.
[24] R. Du, W. Sun, L. Xia, A. Zhao, Y. Yu, L. Zhao, H. Wang, C. Huang, S. Sun, Hypoxia-induced down-regulation of microRNA-34a promotes EMT by targeting the Notch signaling pathway in tubular epithelial cells, PLoS One, 7 (2012) e30771.
[25] S. Granata, G. Zaza, S. Simone, G. Villani, D. Latorre, P. Pontrelli, M. Carella, F.P. Schena, G. Grandaliano, G. Pertosa, Mitochondrial dysregulation and oxidative stress in patients with chronic kidney disease, BMC Genomics, 10 (2009) 388.
[26] C. Sapienza, J. Lee, J. Powell, O. Erinle, F. Yafai, J. Reichert, E.S. Siraj, M. Madaio, DNA methylation profiling identifies epigenetic differences between diabetes patients with ESRD and diabetes patients without nephropathy, Epigenetics, 6 (2011) 20-28.
[27] J.P. Schanstra, M. Bachvarova, E. Neau, J.L. Bascands, D. Bachvarov, Gene expression profiling in the remnant kidney model of wild type and kinin B1 and B2 receptor knockout mice, Kidney Int, 72 (2007) 442-454.
[28] Z. Gai, G. Zhou, T. Gui, S. Itoh, K. Oikawa, K. Uetani, Y. Muragaki, Trps1 haploinsufficiency promotes renal fibrosis by increasing Arkadia expression, J Am Soc Nephrol, 21 (2010) 1468-1476.
[29] S. Zheng, Y. Huang, L. Yang, T. Chen, J. Xu, P.N. Epstein, Uninephrectomy of diabetic OVE26 mice greatly accelerates albuminuria, fibrosis, inflammatory cell infiltration and changes in gene expression, Nephron Exp Nephrol, 119 (2011) e21-32.
[30] M. Praga, E. Hernandez, E. Morales, A.P. Campos, M.A. Valero, M.A. Martinez, M. Leon, Clinical features and long-term outcome of obesity-associated focal segmental glomerulosclerosis, Nephrol Dial Transplant, 16 (2001) 1790-1798.
[31] A. Chagnac, T. Weinstein, A. Korzets, E. Ramadan, J. Hirsch, U. Gafter, Glomerular hemodynamics in severe obesity, Am J Physiol Renal Physiol, 278 (2000) F817-822.
[32] J.M. Nogueira, M.R. Weir, S. Jacobs, D. Breault, D. Klassen, D.A. Evans, S.T. Bartlett, M. Cooper, A study of renal outcomes in obese living kidney donors, Transplantation, 90 (2010) 993-999.
[33] P.O. Attman, O. Samuelsson, P. Alaupovic, Progression of renal failure: role of apolipoprotein B-containing lipoproteins, Kidney Int Suppl, 63 (1997) S98-101.
[34] S. Fiorucci, G. Rizzo, E. Antonelli, B. Renga, A. Mencarelli, L. Riccardi, S. Orlandi, M. Pruzanski, A. Morelli, R. Pellicciari, A farnesoid x receptor-small heterodimer partner regulatory cascade modulates tissue metalloproteinase inhibitor-1 and matrix metalloprotease expression in hepatic stellate cells and promotes resolution of liver fibrosis, J Pharmacol Exp Ther, 314 (2005) 584-595.
[35] X.X. Wang, T. Jiang, Y. Shen, Y. Caldas, S. Miyazaki-Anzai, H. Santamaria, C. Urbanek, N. Solis, P. Scherzer, L. Lewis, F.J. Gonzalez, L. Adorini, M. Pruzanski, J.B. Kopp, J.W. Verlander, M. Levi, Diabetic nephropathy is accelerated by farnesoid X receptor deficiency and inhibited by farnesoid X receptor activation in a type 1 diabetes model, Diabetes, 59 (2010) 2916-2927.
[36] X.X. Wang, T. Jiang, Y. Shen, L. Adorini, M. Pruzanski, F.J. Gonzalez, P. Scherzer, L. Lewis, S. Miyazaki-Anzai, M. Levi, The farnesoid X receptor modulates renal lipid metabolism and diet-induced renal inflammation, fibrosis, and proteinuria, Am J Physiol Renal Physiol, 297 (2009) F1587-1596.

[37] Z. Hu, L. Ren, C. Wang, B. Liu, G. Song, Effect of chenodeoxycholic acid on fibrosis, inflammation and oxidative stress in kidney in high-fructose-fed Wistar rats, Kidney Blood Press Res, 36 (2012) 85-97.
[38] Z. Gai, L. Chu, C. Hiller, D. Arsenijevic, C.A. Penno, J.P. Montani, A. Odermatt, G.A. Kullak-Ublick, Effect of chronic renal failure on the hepatic, intestinal, and renal expression of bile acid transporters, Am J Physiol Renal Physiol, 306 (2014) F130-137.
[39] D. Jung, G.A. Kullak-Ublick, Hepatocyte nuclear factor 1 alpha: a key mediator of the effect of bile acids on gene expression, Hepatology, 37 (2003) 622-631.
[40] K. Popowski, J.J. Eloranta, M. Saborowski, M. Fried, P.J. Meier, G.A. Kullak-Ublick, The human organic anion transporter 2 gene is transactivated by hepatocyte nuclear factor-4 alpha and suppressed by bile acids, Mol Pharmacol, 67 (2005) 1629-1638.
[41] P. Fickert, E. Krones, M.J. Pollheimer, A. Thueringer, T. Moustafa, D. Silbert, E. Halilbasic, M. Yang, H. Jaeschke, G. Stokman, R.G. Wells, K. Eller, A.R. Rosenkranz, G. Eggertsen, C.A. Wagner, C. Langner, H. Denk, M. Trauner, Bile acids trigger cholemic nephropathy in common bile-duct-ligated mice, Hepatology, 58 (2013) 2056-2069.
[42] A.E. Decleves, Z. Zolkipli, J. Satriano, L. Wang, T. Nakayama, M. Rogac, T.P. Le, J.L. Nortier, M.G. Farquhar, R.K. Naviaux, K. Sharma, Regulation of lipid accumulation by AMK-activated kinase in high fat diet-induced kidney injury, Kidney international, 85 (2014) 611-623.
[43] P. Delanaye, L. Weekers, B.E. Dubois, E. Cavalier, O. Detry, J.P. Squifflet, J.M. Krzesinski, Outcome of the living kidney donor, Nephrol Dial Transplant, 27 (2012) 41-50.
[44] P.J. Westenend, Y.A. Nooyen, J.A. van der Krogt, P. van Brummelen, J.J. Weening, Functional and structural determinants of glomerulosclerosis in the fawn-hooded rat, Eur J Clin Invest, 22 (1992) 391-395.
[45] V. Ninichuk, O. Kulkarni, S. Clauss, H. Anders, Tubular atrophy, interstitial fibrosis, and inflammation in type 2 diabetic db/db mice. An accelerated model of advanced diabetic nephropathy, Eur J Med Res, 12 (2007) 351-355.
[46] S.D. Navaneethan, H. Yehnert, F. Moustarah, M.J. Schreiber, P.R. Schauer, S. Beddhu, Weight loss interventions in chronic kidney disease: a systematic review and meta-analysis, Clin J Am Soc Nephrol, 4 (2009) 1565-1574.
[47] M. Nangaku, Y. Izuhara, N. Usuda, R. Inagi, T. Shibata, S. Sugiyama, K. Kurokawa, C. van Ypersele de Strihou, T. Miyata, In a type 2 diabetic nephropathy rat model, the improvement of obesity by a low calorie diet reduces oxidative/carbonyl stress and prevents diabetic nephropathy, Nephrol Dial Transplant, 20 (2005) 2661-2669.
[48] S. Ohtomo, Y. Izuhara, M. Nangaku, T. Dan, S. Ito, C. van Ypersele de Strihou, T. Miyata, Body weight control by a high-carbohydrate/low-fat diet slows the progression of diabetic kidney damage in an obese, hypertensive, type 2 diabetic rat model, J Obes, 2010 (2010).
[49] C.L. Davis, M. Cooper, The state of U.S. living kidney donors, Clin J Am Soc Nephrol, 5 (2010) 1873-1880.

Figure 1

Click here to download high resolution image

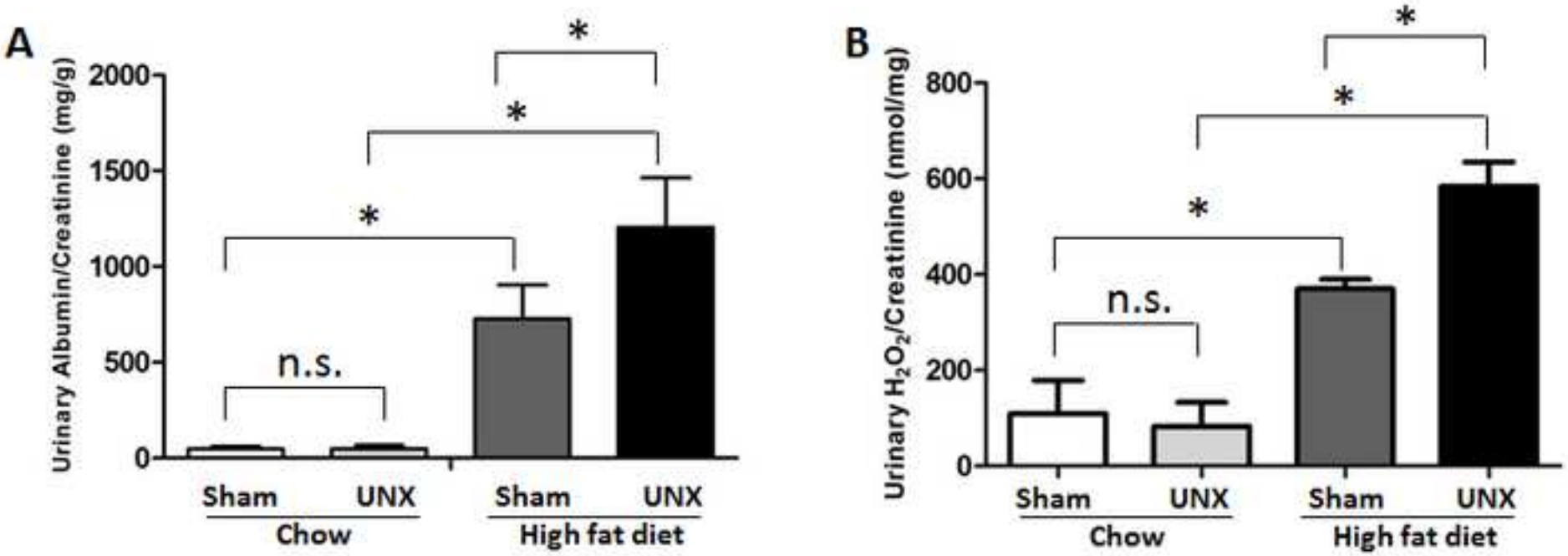

Figure 2

Click here to download high resolution image

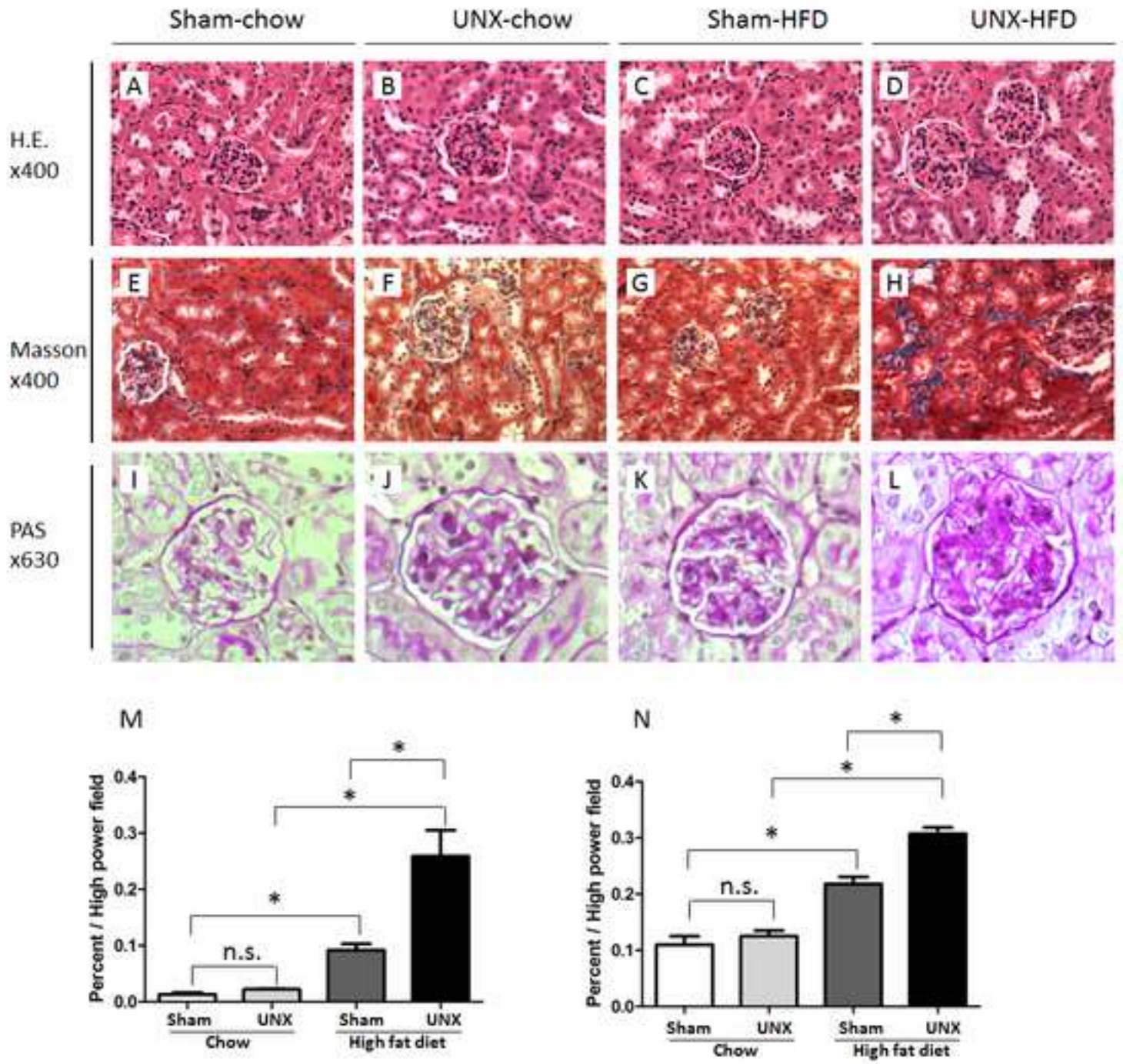

Figure 3

Click here to download high resolution image

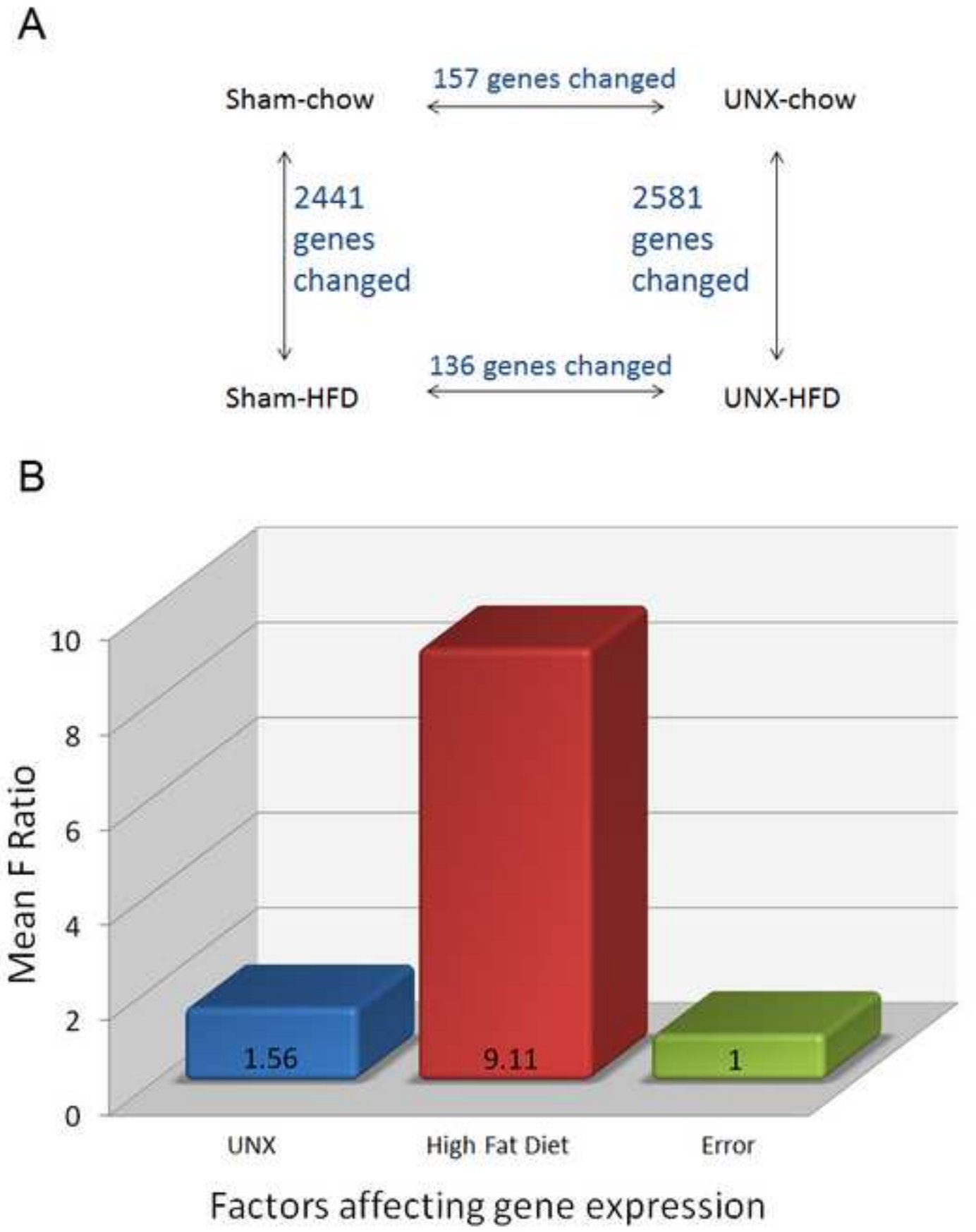

Figure 4

Click here to download high resolution image

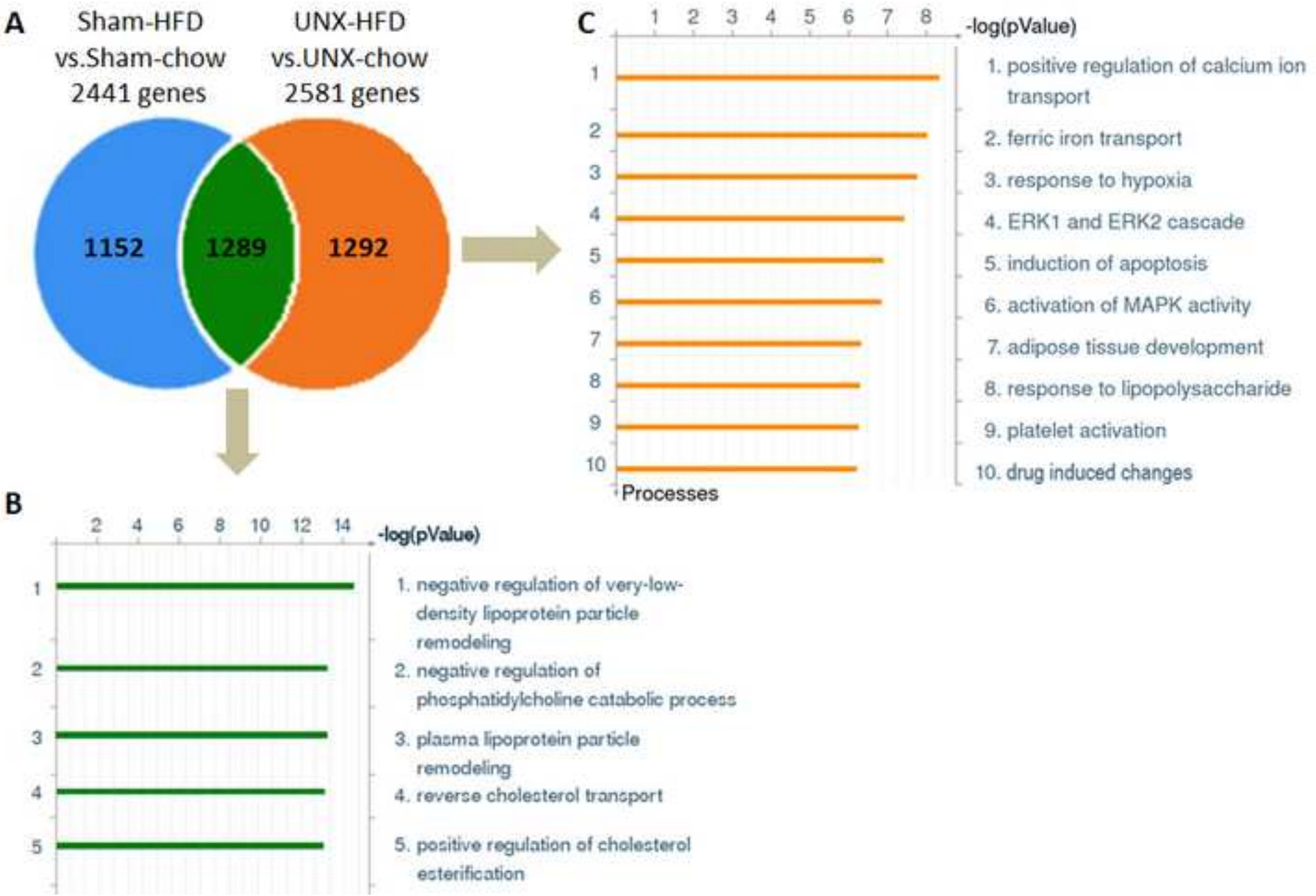

Figure 5

Click here to download high resolution image

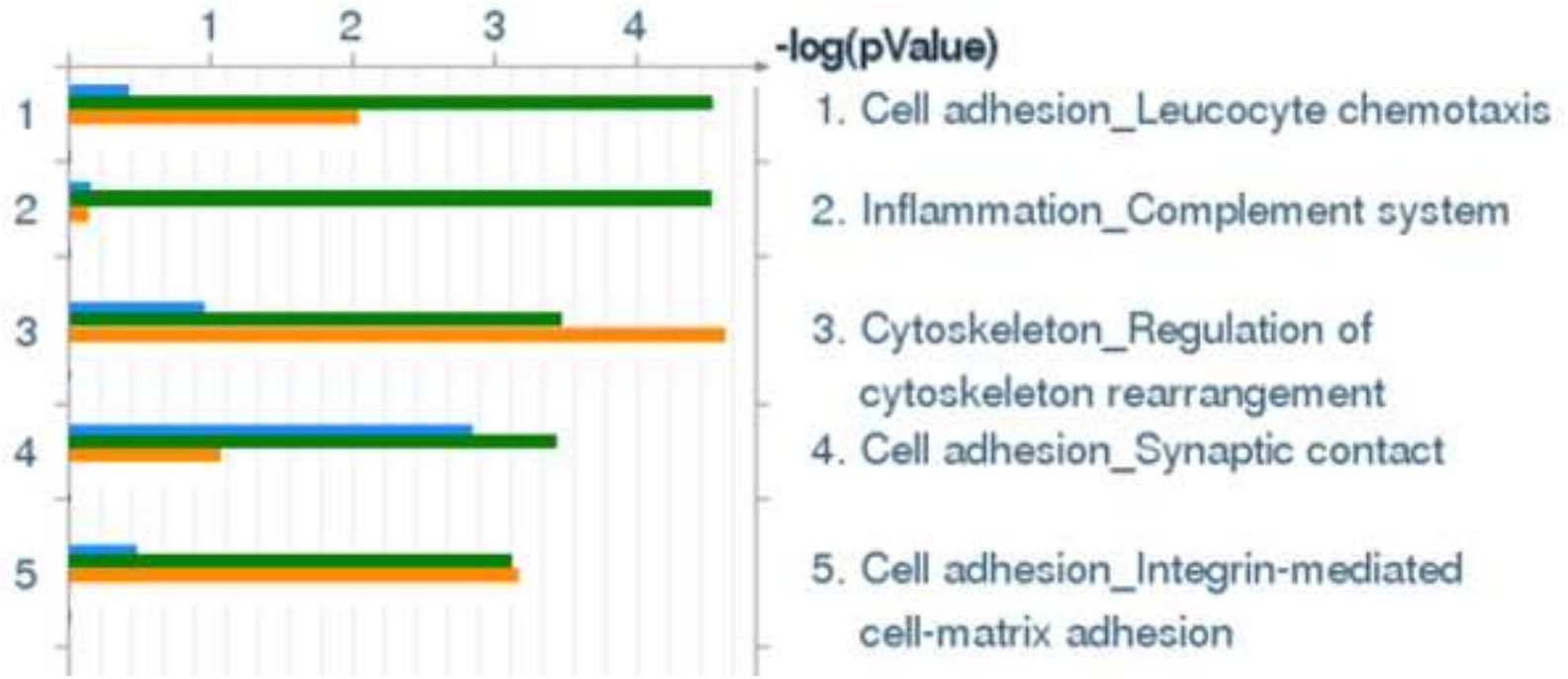

Figure 6

Click here to download high resolution image

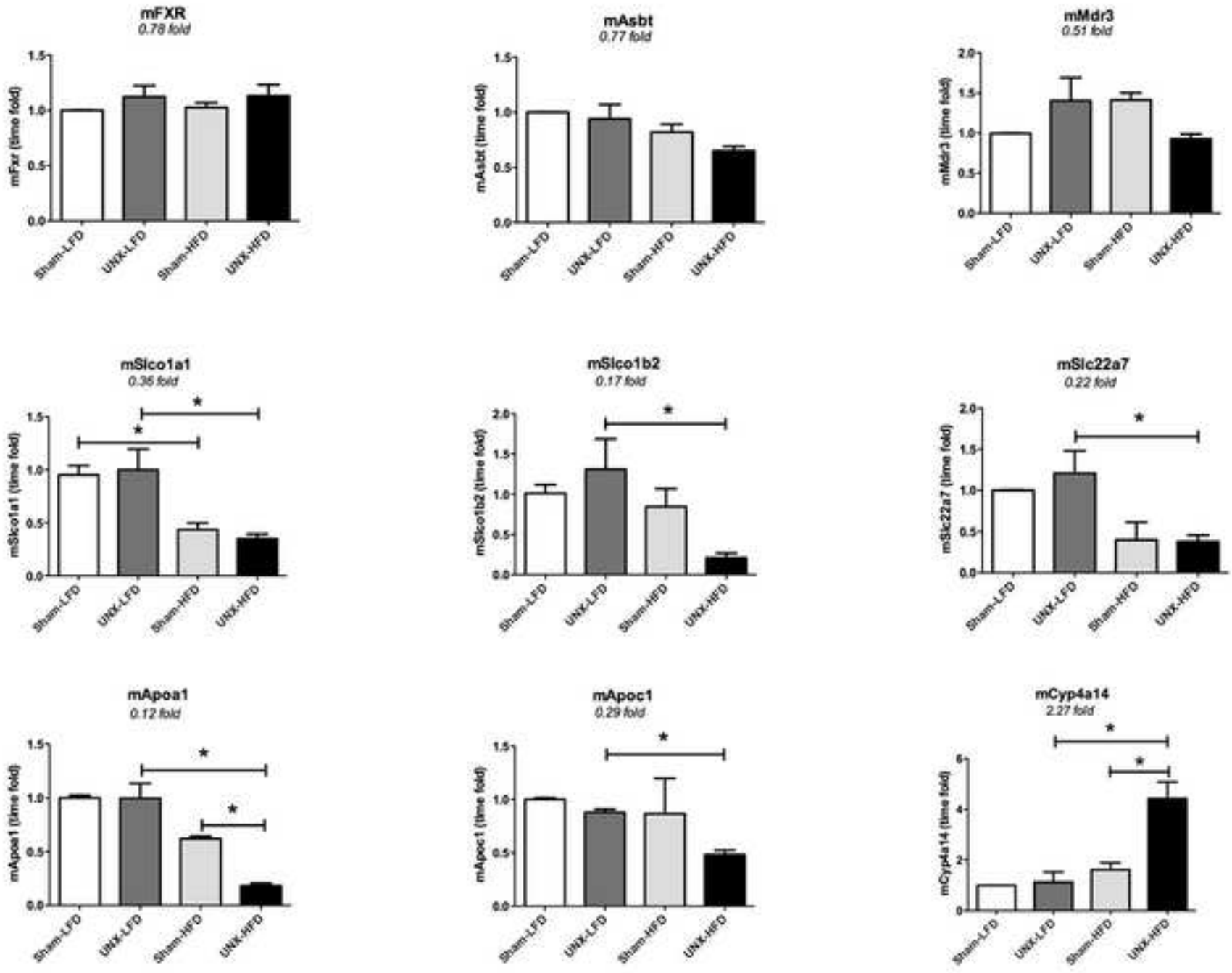

Figure 7

Click here to download high resolution image

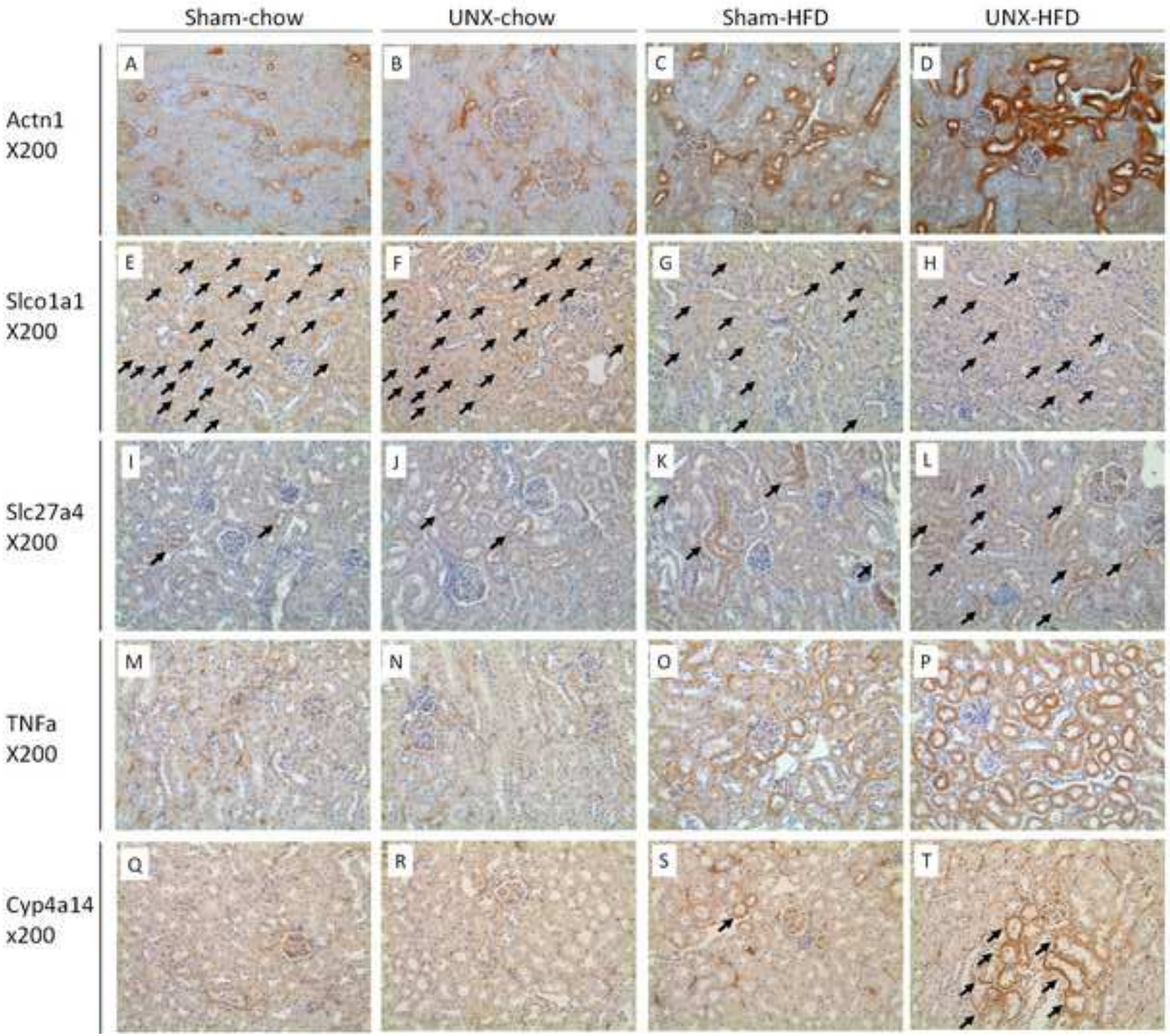

Supplementary Material (for online publication)

Click here to download Supplementary Material (for online publication): Table S1.xlsx

NAME	Fold Chang	P-Value	GENE_SYM	GENE_NAM	GO_ID
A_51_P481	1.761865	0.001945	Dram1	DNA-dama	GO:0003674(molecular_function)|GO:000557
A_65_P076	8.103457	0.00305			
A_51_P448	1.839305	0.044903	Elf4	E74-like fa	GO:0001787(natural killer cell proliferation)|G
A_55_P225	6.556071	0.010778	Mpp2	membrane	GO:0005515(protein binding)|GO:0009986(ce
A_55_P217	2.398375	0.02153			
A_55_P216	2.817647	0.042214	2300005B0	RIKEN cDN	GO:0003674(molecular_function)|GO:000557
A_55_P214	4.377593	1.92E-04	Pex5l	peroxisom	GO:0000268(peroxisome targeting sequence b
A_55_P200	3.848433	0.017959	Dzip1	DAZ intera	GO:0005515(protein binding)|GO:0005622(in
A_55_P208	2.921548	0.003579	Hpca	hippocalcir	GO:0003779(actin binding)|GO:0005509(calci
A_55_P228	3.445533	0.002752	4930478P2	RIKEN cDNA 4930478P22 gene	
A_55_P218	2.556891	0.001853			
A_52_P683	1.827733	0.002737	Tbc1d9	TBC1 dom	GO:0003674(molecular_function)|GO:000509
A_66_P132	2.814476	8.64E-04			
A_55_P210	1.816696	0.028917	Ggn	gametogen	GO:0005515(protein binding)|GO:0005634(nu
A_51_P135	3.357786	0.008657	Coch	coagulatio	GO:0003674(molecular_function)|GO:000557
A_55_P217	2.064302	0.00834	Nfasc	neurofasci	GO:0002175(protein localization to paranode
A_55_P202	1.831174	0.020929	C87414	expressed	GO:0003674(molecular_function)|GO:000557
A_52_P223	4.00476	4.47E-04	Zfp37	zinc finger	GO:0003676(nucleic acid binding)|GO:000367
A_52_P487	1.946543	0.002308	Thnsl2	threonine s	GO:0004795(threonine synthase activity)|GO
A_51_P293	2.06703	0.042471	Plekho2	pleckstrin h	GO:0003674(molecular_function)|GO:000554
A_55_P214	1.927308	0.006145			
A_55_P206	1.823752	0.007865	Ush1g	Usher synd	GO:0005515(protein binding)|GO:0005737(cy
A_55_P206	2.078934	0.029772	Defa1	defensin, a	GO:0005576(extracellular region)|GO:000561
A_55_P200	1.778136	0.002865	Ovch2	ovochymas	GO:0003824(catalytic activity)|GO:0004252(s
A_51_P242	1.746102	0.00591	Lat2	linker for a	GO:0005622(intracellular)|GO:0005886(plasm
A_52_P809	3.053202	0.03286	Zfp36	zinc finger	GO:0000122(negative regulation of transcript
A_55_P206	1.776402	0.00353	Fgd5	FYVE, RhoG	GO:0003674(molecular_function)|GO:000508
A_52_P536	2.145072	0.005903	Hpgds	hematopoi	GO:0000287(magnesium ion binding)|GO:000
A_51_P341	2.14183	0.030757	Mmp2	matrix met	GO:0001525(angiogenesis)|GO:0001541(ovar
A_55_P204	2.051177	3.70E-05	Smn1	survival mo	GO:0003723(RNA binding)|GO:0005634(nucle
A_55_P202	4.154113	0.01021	Ccdc169	coiled-coil	GO:0003674(molecular_function)|GO:000557
A_55_P237	1.994081	0.020853	Kcnma1	potassium	GO:0000166(nucleotide binding)|GO:000166
A_51_P427	2.558353	0.001334	Lacc1	laccase (mu	GO:0003674(molecular_function)|GO:000557
A_52_P118	1.903089	0.002617	Pex19	peroxisom	GO:0005515(protein binding)|GO:0005634(nu
A_51_P389	2.323341	6.58E-04	Scrt2	scratch hor	GO:0003676(nucleic acid binding)|GO:000367
A_55_P196	2.427879	0.005664			
A_55_P195	2.40682	0.002187			
A_55_P203	1.927606	0.009197	Speer5-ps1	spermatogenesis associated glutamate (E)-rich protein 5,	
A_52_P523	2.352239	0.005006	Sh2d6	SH2 domai	GO:0003674(molecular_function)|GO:000557
A_55_P216	3.301989	0.039021	Gm10220	predicted g	GO:0003674(molecular_function)|GO:000557
A_55_P215	2.062939	0.020058	Mcm9	minichrom	GO:0000166(nucleotide binding)|GO:000072
A_55_P201	2.068399	0.005047	Agbl4	ATP/GTP bi	GO:0004180(carboxypeptidase activity)|GO:0
A_55_P212	1.7195	0.003445	Pdcd1lg2	programme	GO:0005515(protein binding)|GO:0005886(pl
A_55_P199	2.171455	0.009334			
A_66_P129	2.49522	0.023319	Ngb	neuroglobi	GO:0005344(oxygen transporter activity)|GO:
A_55_P195	4.146521	0.002995			

Supplementary Material (for online publication)

Click here to download Supplementary Material (for online publication): Table S2.xlsx

NAME	Fold Chang	P-Value	GENE_SYM	GENE_NAM	GO_ID
A_65_P076	8.307668	0.010207			
A_55_P216	3.722401	0.001399	2300005B0	RIKEN cDN	GO:0003674(molecular_function)|GO:000557
A_55_P217	2.533281	0.001827			
A_55_P200	3.672292	0.003	Dzip1	DAZ intera	GO:0005515(protein binding)|GO:0005622(in
A_55_P214	2.597939	0.003074	Pex5l	peroxisom	GO:0000268(peroxisome targeting sequence
A_55_P215	2.153574	7.91E-04	Cpne5	copine V	GO:0003674(molecular_function)|GO:000815
A_55_P210	1.778609	0.001725	Ggn	gametogen	GO:0005515(protein binding)|GO:0005634(nu
A_55_P217	2.018861	4.41E-04	Nfasc	neurofascir	GO:0002175(protein localization to paranode
A_52_P487	1.781307	0.001765	Thnsl2	threonine s	GO:0004795(threonine synthase activity)|GO
A_55_P206	1.755812	0.001707	Ush1g	Usher synd	GO:0005515(protein binding)|GO:0005737(cy
A_55_P214	1.916453	6.81E-04			
A_52_P609	2.420619	0.037332	Eln	elastin	GO:0001974(blood vessel remodeling)|GO:00
A_55_P202	3.849947	0.005937	Ccdc169	coiled-coil	GO:0003674(molecular_function)|GO:000557
A_51_P389	2.134217	8.76E-04	Scrt2	scratch hor	GO:0003676(nucleic acid binding)|GO:000367
A_51_P193	2.57158	2.35E-04	Slc25a25	solute carri	GO:0005509(calcium ion binding)|GO:000573
A_55_P218	1.992609	5.60E-04	Tmem28	transmemb	GO:0003674(molecular_function)|GO:000557
A_55_P198	2.217834	0.034632	Cxx1a	CAAX box 1	GO:0003674(molecular_function)|GO:000557
A_55_P195	2.286358	3.58E-04			
A_55_P198	1.922985	0.002823			
A_55_P199	1.994891	0.002202			
A_55_P226	1.996629	0.008285	9330199G1	RIKEN cDNA 9330199G10 gene	
A_51_P348	1.804534	0.035817	Slc38a7	solute carri	GO:0005290(L-histidine transmembrane trans
A_55_P198	2.872486	0.011269	Bcl11a	B cell CLL/l	GO:0003676(nucleic acid binding)|GO:000371
A_55_P213	3.956673	0.030769	H2-M2	histocompa	GO:0003674(molecular_function)|GO:000815
A_52_P680	3.24088	0.021368	Ace	angiotensir	GO:0001822(kidney development)|GO:00024
A_55_P206	1.990991	0.034442	Colq	collagen-lik	GO:0005581(collagen)|GO:0008201(heparin b
A_55_P208	2.234258	0.002157			
A_51_P438	4.210516	0.012624	Gpnmb	glycoprotei	GO:0005178(integrin binding)|GO:0005887(ir
A_55_P203	1.882102	0.019196	Slc5a4a	solute carri	GO:0005215(transporter activity)|GO:000681
A_55_P217	9.622099	2.87E-06			
A_55_P210	2.368195	1.26E-04	Utf1	undifferent	GO:0003713(transcription coactivator activity
A_51_P106	1.706934	0.026615	Celf3	CUGBP, Ela	GO:0000166(nucleotide binding)|GO:000038
A_66_P107	1.711738	0.049891	3300005D0	RIKEN cDNA 3300005D01 gene	
A_51_P341	1.972925	2.97E-05	Tsc22d1	TSC22 dom	GO:0003700(sequence-specific DNA binding t
A_51_P102	3.309079	7.97E-05	Tmem225	transmemb	GO:0003674(molecular_function)|GO:000557
A_51_P276	3.36924	1.05E-04	Olfr1350	olfactory re	GO:0004871(signal transducer activity)|GO:0
A_55_P196	2.140484	0.032632	Carm1	coactivator	GO:0003420(regulation of growth plate cartila
A_55_P211	2.162356	0.003166	Pvalb	parvalbumi	GO:0005509(calcium ion binding)|GO:000563
A_55_P197	1.905833	0.001541	Nlrp12	NLR family,	GO:0000166(nucleotide binding)|GO:000367
A_55_P210	3.691839	3.89E-04	Scn11a	sodium cha	GO:0001518(voltage-gated sodium channel c
A_55_P212	1.96411	0.00218			GO:0000079(regulation of cyclin-dependent p
A_52_P175	1.973904	0.040809	A4gnt	alpha-1,4-N	GO:0005575(cellular_component)|GO:00064
A_55_P199	1.85163	0.005387			
A_55_P205	1.750975	0.006405	Mall	mal, T cell	GO:0000139(Golgi membrane)|GO:0003674(r
A_55_P205	1.722417	0.013915	Foxf1	forkhead b	GO:0000122(negative regulation of transcript
A_55_P202	1.759163	0.049787	Dyrk1b	dual-specif	GO:0000166(nucleotide binding)|GO:000371

Supplementary Material (for online publication)

Click here to download Supplementary Material (for online publication): Table S3.xlsx

measurem	Fold Chang	Log2Ratio	P-Value	GENE_SYM	GENE_NAM	GO_ID	Selection
A_65_P076	8.307668	3.054444	0.010207				1
A_55_P216	3.722401	1.896234	0.001399	2300005BC	RIKEN cDN	GO:000367	1
A_55_P217	2.533281	1.341007	0.001827				1
A_55_P200	3.672292	1.876681	0.003	Dzip1	DAZ intera	GO:000551	1
A_55_P214	2.597939	1.377367	0.003074	Pex5l	peroxisom	GO:000026	1
A_55_P210	1.778609	0.830749	0.001725	Ggn	gametogen	GO:000551	1
A_55_P217	2.018861	1.013542	4.41E-04	Nfasc	neurofascir	GO:000217	1
A_52_P487	1.781307	0.832936	0.001765	Thnsl2	threonine s	GO:000479	1
A_55_P206	1.755812	0.812139	0.001707	Ush1g	Usher synd	GO:000551	1
A_55_P214	1.916453	0.938439	6.81E-04				1
A_55_P202	3.849947	1.944838	0.005937	Ccdc169	coiled-coil	GO:000367	1
A_51_P389	2.134217	1.093707	8.76E-04	Scrt2	scratch hor	GO:000367	1
A_55_P195	2.286358	1.193051	3.58E-04				1
A_55_P199	1.994891	0.99631	0.002202				1
A_55_P198	2.872486	1.5223	0.011269	Bcl11a	B cell CLL/l	GO:000367	1
A_52_P680	3.24088	1.696386	0.021368	Ace	angiotensir	GO:000182	1
A_55_P208	2.234258	1.159796	0.002157				1
A_55_P203	1.882102	0.912345	0.019196	Slc5a4a	solute carri	GO:000521	1
A_55_P217	9.622099	3.266352	2.87E-06				1
A_55_P210	2.368195	1.243788	1.26E-04	Utf1	undifferent	GO:000371	1
A_51_P102	3.309079	1.72643	7.97E-05	Tmem225	transmemb	GO:000367	1
A_51_P276	3.36924	1.752423	1.05E-04	Olfr1350	olfactory re	GO:000487	1
A_55_P211	2.162356	1.112604	0.003166	Pvalb	parvalbumi	GO:00055C	1
A_55_P197	1.905833	0.930422	0.001541	Nlrp12	NLR family,	GO:000016	1
A_55_P210	3.691839	1.88434	3.89E-04	Scn11a	sodium cha	GO:000151	1
A_52_P175	1.973904	0.981052	0.040809	A4gnt	alpha-1,4-N	GO:000557	1
A_55_P199	1.85163	0.888796	0.005387				1
A_55_P205	1.750975	0.808158	0.006405	Mall	mal, T cell	GO:000013	1
A_55_P202	1.759163	0.814889	0.049787	Dyrk1b	dual-specif	GO:000016	1
A_55_P213	2.538173	1.34379	1.63E-04				1
A_55_P205	1.831663	0.873154	0.004644	Olfr1382	olfactory re	GO:000487	1
A_51_P110	1.922133	0.942708	8.52E-04	Wwox	WW domai	GO:000016	1
A_55_P211	1.719641	0.782107	0.030415	Hyls1	hydroletha	GO:000367	1
A_51_P362	3.192259	1.674578	2.33E-04	Olfr1307	olfactory re	GO:000487	1
A_55_P212	4.121563	2.043191	2.46E-04	Zfp36l3	zinc finger	GO:000028	1
A_55_P213	7.046661	2.81694	1.14E-04	Sva	seminal ves	GO:000561	1
A_51_P360	1.81645	0.861122	5.47E-04	Ocstamp	osteoclast	GO:000367	1
A_55_P202	2.310471	1.208187	0.002324	Gm7104	REX1, RNA exonuclease		1
A_55_P196	1.71581	0.77889	0.013315				1
A_55_P204	2.056166	1.039957	0.001863	Rbp3	retinol binc	GO:000557	1
A_55_P195	2.041394	1.029554	2.32E-05	Slit1	slit homolo	GO:00051C	1
A_55_P210	2.455452	1.295988	8.34E-05	Ephb6	Eph recept	GO:000016	1
A_55_P203	2.81023	1.490688	0.00943	4933427D(	RIKEN cDN	GO:000367	1
A_55_P218	1.826778	0.869302	0.003106	Sh3bp1	SH3-domai	GO:000509	1
A_52_P649	1.961118	0.971677	0.003811	Smyd3	SET and M	GO:000557	1
A_66_P129	3.379755	1.756919	1.33E-04	D030024E(	RIKEN cDNA	D030024E	1
GE_BrightC	2.262746	1.178075	0.005464				1
A_55_P213	2.09655	1.068017	6.36E-04				1
A_51_P378	3.002366	1.5861	0.00123	Coq3	coenzyme	GO:000439	1

Supplementary Material (for online publication)

Click here to download Supplementary Material (for online publication): Table S4.xlsx

measurem	Fold Chang	Log2Ratio	P-Value	GENE_SYM	GENE_NAM	GO_ID	Selection
A_55_P215	2.153574	1.106733	7.91E-04	Cpne5	copine V	GO:000367	1
A_52_P609	2.420619	1.275376	0.037332	Eln	elastin	GO:000197	1
A_51_P193	2.57158	1.362655	2.35E-04	Slc25a25	solute carri	GO:00055C	1
A_55_P218	1.992609	0.994659	5.60E-04	Tmem28	transmemb	GO:000367	1
A_55_P198	2.217834	1.149152	0.034632	Cxx1a	CAAX box 1	GO:000367	1
A_55_P198	1.922985	0.943348	0.002823				1
A_55_P226	1.996629	0.997566	0.008285	9330199G1	RIKEN cDNA	9330199C	1
A_51_P348	1.804534	0.851626	0.035817	Slc38a7	solute carri	GO:000529	1
A_55_P213	3.956673	1.984288	0.030769	H2-M2	histocompa	GO:000367	1
A_55_P206	1.990991	0.993486	0.034442	Colq	collagen-lik	GO:000558	1
A_51_P438	4.210516	2.073997	0.012624	Gpnmb	glycoprotei	GO:000517	1
A_51_P106	1.706934	0.771407	0.026615	Celf3	CUGBP, Ela	GO:000016	1
A_66_P107	1.711738	0.775462	0.049891	3300005D0	RIKEN cDNA	3300005D	1
A_51_P341	1.972925	0.980336	2.97E-05	Tsc22d1	TSC22 dom	GO:00037C	1
A_55_P196	2.140484	1.097937	0.032632	Carm1	coactivator	GO:000342	1
A_55_P212	1.96411	0.973876	0.00218			GO:000007	1
A_55_P205	1.722417	0.784435	0.013915	Foxf1	forkhead b	GO:000012	1
A_55_P218	1.953938	0.966385	0.001928	Cacng6	calcium cha	GO:000521	1
A_55_P205	3.059473	1.613283	4.04E-04	Olfr1382	olfactory re	GO:000487	1
A_55_P218	1.961906	0.972256	6.51E-05	Chrnb4	cholinergic	GO:00015C	1
A_51_P347	3.236079	1.694247	0.027118	Actn1	actinin, alp	GO:000172	1
A_55_P201	1.918571	0.940032	0.016742				1
A_51_P210	1.812894	0.858295	0.018748	Nudt18	nudix (nucl	GO:000028	1
A_55_P197	3.358355	1.747755	2.41E-04	BC089597	cDNA sequ	GO:000367	1
A_55_P235	2.895082	1.533604	7.14E-04	DXErtd223	DNA segment, Chr X, E		1
A_55_P203	2.601975	1.379607	0.011546				1
A_55_P218	1.875482	0.907261	0.003458	Mettl7a3	methyltran	GO:000367	1
A_66_P137	3.208132	1.681733	5.78E-04	A730045E1	RIKEN cDN	GO:000367	1
A_55_P197	2.403847	1.265345	0.001814				1
A_55_P214	1.744885	0.803132	3.86E-04	Gm5101	predicted g	GO:000367	1
A_55_P210	1.765495	0.820072	0.035157	Ache	acetylcholi	GO:000191	1
A_52_P483	2.915783	1.543883	0.010482	Ms4a1	membrane	GO:000515	1
A_55_P210	2.148441	1.10329	0.027633	Ache	acetylcholi	GO:000191	1
A_55_P202	1.897563	0.924148	0.007127	Leng8	leukocyte r	GO:000557	1
A_55_P201	1.736069	0.795825	1.11E-04	Kif17	kinesin fam	GO:000016	1
A_55_P206	2.057469	1.040871	0.002844				1
A_55_P208	2.016144	1.011599	1.01E-04				1
A_55_P195	1.733411	0.793614	0.014242				1
A_66_P110	1.839291	0.87915	1.64E-04	Tmem91	transmemb	GO:000367	1
A_55_P213	1.748813	0.806376	0.017496	C8g	complemer	GO:000184	1
A_55_P217	2.070768	1.050166	0.002247				1
A_55_P195	2.799554	1.485197	0.001862				1
A_55_P241	1.765981	0.82047	0.00345	4930581F2	RIKEN cDN	GO:000367	1
A_55_P213	1.862149	0.896969	4.35E-04	Cnn3	calponin 3,	GO:000377	1
A_55_P209	2.402795	1.264713	0.012046	Msh4	mutS homc	GO:000016	1
A_55_P200	2.384703	1.253809	0.035638	Armc3	armadillo r	GO:000367	1

Supplementary Material (for online publication)

Click here to download Supplementary Material (for online publication): Table S5.xlsx

Formula

#D12331		gm%	kcal%
Protein		23	16.4
Carbohydrate		35.5	25.5
Fat		35.8	58
	Total		100
	kcal/gm	5.56	

Ingredient	gm	kcal
Casein, 30 Mesh	228	912
DL-Methionine	2	0
Maltodextrin 10	170	680
Corn Starch	0	0
Sucrose	175	700
Soybean Oil	25	225
Conconut Oil	333.5	3001.5
Mineral Mix	40	0
Sodium Bicarbonate	10.5	0
Potassium Citrate	4	0
Vitamin Mix	10	40
Choline Bitartrate	2	0
FD&C Red Dye	0.1	0
Total	1000.1	5558.5

Thin layer chromatography

For the analysis of lipid, frozen kidney tissue samples (4 % wt/vol) were homogenized with a tight fitting glass-teflon homogenizer at full speed in 250 mM sucrose, 10 mM Tris/HCl pH 7.4 (supplemented with Complete Mini protease inhibitors from Roche). 1 mg of homogenate (BCA protein determination kit from Interchim, Montlucon, France) was extracted as determined as described in [1]. The extracted lipids were analyzed for phospholipid and cholesterol content by thin-layer chromatography as described in [2]. Determination of total phospholipids was performed as published in [3].

References

[1] E.G. Bligh, W.J. Dyer, A rapid method of total lipid extraction and purification, Canadian journal of biochemistry and physiology, 37 (1959) 911-917.
[2] M.G. Ismair, S. Hausler, C.A. Stuermer, C. Guyot, P.J. Meier, J. Roth, B. Stieger, ABC-transporters are localized in caveolin-1-positive and reggie-1-negative and reggie-2-negative microdomains of the canalicular membrane in rat hepatocytes, Hepatology, 49 (2009) 1673-1682.
[3] G. Rouser, S. Fkeischer, A. Yamamoto, Two dimensional then layer chromatographic separation of polar lipids and determination of phospholipids by phosphorus analysis of spots, Lipids, 5 (1970) 494-496.

Supplementary Figure (for online publication)

Click here to download high resolution image